applied optics

Nonnull interferometric testing of spherical gratings under Littrow conditions with opposite diffraction orders

Weijian Liu,[1] Qun Yuan,[1] Ruoyan Wang,[1] Wen Ji,[1] YingZe Xue,[1] Jun Ma,[1] Lingjie Wang,[2] and Zhishan Gao[1,*]

[1]School of Electronic and Optical Engineering, Nanjing University of Science and Technology, Nanjing 210094, China
[2]Key Laboratory of Optical System Advanced Manufacturing Technology, Changchun Institute of Optics, Fine Mechanics and Physics, Chinese Academy of Sciences, Changchun 130033, China
*Corresponding author: zhishgao@njust.edu.cn

Received 20 May 2020; revised 17 June 2020; accepted 18 June 2020; posted 18 June 2020 (Doc. ID 398003); published 17 July 2020

Diffracted wavefront measurements are qualitative and comprehensive verifications for the spherical grating that was manufactured to specifications. Direct interferometric testing of the diffracted wavefront is convenient and implemented by tilting the spherical grating at a Littrow angle to obtain autoreflection and then results in a nonnull interferometric testing configuration. The diffracted wavefront of the spherical grating contains not only wavefront errors induced by the manufacturing imperfections but also inherent wavefront contributions from the autoreflection testing setup. The magnitudes of the latter are affected by both the spherical substrate and the groove pattern. Through the analysis of geometric aberrations of spherical gratings, the groove pattern contributions are demonstrated to be contrary for the opposite diffraction orders. A nonnull interferometric testing of spherical gratings is proposed without foreknowledge of the groove pattern, in which the wavefront errors contributed only by the manufacturing imperfections are derived from dual measurements under Littrow conditions with opposite diffraction orders. Simulations are implemented for varied line spacing (VLS) spherical gratings with an F-number slower than 1.5 and groove density varying from 150 to 300 lp/mm, and the residual error less than 0.004λ RMS is obtained. The residual misalignment error after conventionally removing defocus and tilt is further analyzed and discussed. A VLS grating in which the NA is 0.13 and groove density is 200 lp/mm is chosen as an experimental sample, and the diffracted wavefront error with 0.018λ RMS is obtained.

https://doi.org/10.1364/AO.398003

1. INTRODUCTION

Spherical gratings fabricated on either concave substrates or convex substrates have been widely utilized in hyperspectral imaging spectrometers to take the advantage of providing both focusing and dispersing properties [1–4]. The departure from the ideal spherical substrate, as well as the deviation from the theoretical groove spacing, depth, and parallelism, will introduce aberrations in the diffracted wavefront [5,6]. Afterward, the aberrated diffracted wavefront from the spherical grating will directly affect the imaging quality and the spectral resolution. Therefore, the wavefront testing of the diffracted beam is a comprehensive performance evaluation method for the spherical gratings.

Considering the characteristic of groove spacing, spherical gratings are divided into two categories. One is the classical spherical grating whose grooves, when projected onto the tangent plane, forms a set of straight equally spaced lines. The other is the spherical grating with variations in curvature and spacing of the grooves. Wavefront testing for a flat grating can be done conveniently by placing it at the Littrow angle in a commercial interferometer [7]. Under this condition, autoreflection from the grating is established for the principal rays. However, the off-axis incident rays will not propagate along the original path after diffracted from the spherical grating at the Littrow angle, and will cause the noncoincidence of the meridian focus plane and the sagittal focus plane. Therefore, the wavefront aberrations under Littrow conditions increase the testing difficulty. Confronting the toric characteristic of the wavefront diffracted from a concave grating, a similar toric wavefront reconstructed by a lensless Fourier-transform-type hologram was proposed as a reference wavefront. And the good match between the reference wavefront and diffracted wavefront of the concave grating was obtained [8]. In addition, the method that compares the measured wavefront and computer-modeled diffracted wavefront of the grating was proposed to monitor the quality of concave gratings [9]. A hologram was used in the wavefront testing

layout to compensate the dominant astigmatic aberration of the grating, and the difference between the computer modeled and the experimental captured interferograms indicated the fabrication errors of the grating. A unique hologram is necessary for each grating; so this method is not cost-effective.

Grating testing under its working condition has also been considered to obtain a null interferometric testing configuration. To test a constant line spacing convex grating, a nulling wavefront metrology method was designed with a custom Offner-type layout under similar condition as in use in the spectrometer [10]. However, the optical layout is complex and necessitates the sophisticated alignment. The constant line spacing convex grating was then preferred to be tested under Littrow conditions due to its ease to execute, and the result was acquired after roughly removing piston, tilt, defocus, and astigmatism from the measured data. The tested diffracted wavefront error was consistent with the testing result under its working condition [11]. In Ref. [11], a varied line spacing (VLS) grating was also tested under Littrow conditions, and the residual cubic behavior in the testing results induced by groove pattern contributions should be calculated and further removed from the measured data. The calculation of the groove pattern contributions for VLS spherical gratings requires knowledge of the specific equation of the groove distribution and complicated calculations. Moreover, there are some replicated gratings with only the known specifications as radius of curvature, effective aperture, and groove density at its vertex, but unknown groove distributions. However, the wavefront testing of this type of replicated grating is still in demand.

The testing of spherical gratings under Littrow conditions without using extra compensation components is a general way. Consequently, the elimination of groove pattern contributions from the measured data for VLS spherical gratings with unknown groove distributions is a crucial advance and is proposed and elaborated in this paper. In this paper, based on the aberration analysis of the diffracted wavefront of the spherical grating placed at its Littrow angle in the interferometric testing setup, we present a simple method to directly test wavefront error of spherical gratings. In Section 2, we discuss the theory of the diffracted wavefront of spherical gratings and the analysis of the testing layout of spherical gratings under Littrow conditions. In Section 3, the dual measurements method and the corresponding processing procedure are elaborated on. Section 4 shows the simulation results of the nonnull interferometric testing method and the misalignment aberrations analysis. The experimental results of a VLS concave grating are presented in Section 5. Some concluding remarks are drawn in Section 6.

2. DIFFRACTED WAVEFRONT ANALYSIS

A. Diffracted Wavefront of Spherical Gratings

The diffracted wavefront of spherical gratings is generally demonstrated by geometric analysis. The theory has been widely used in grating spectrometer design [12,13]. The wavefront W is expressed as the sum of substrate surface contributions W_M and groove pattern contributions W_H,

$$\begin{aligned} W &= W_M + W_H \\ &= \sum_{i=0}^{\infty}\sum_{j=0}^{\infty} M_{ij}x^i y^j + \sum_{i=0}^{\infty}\sum_{j=0}^{\infty} H_{ij}x^i y^j \\ &= \sum_{i=0}^{\infty}\sum_{j=0}^{\infty} (M_{ij} + H_{ij})x^i y^j, \end{aligned} \tag{1}$$

where W_M and W_H are expressed as the power series expansion in terms of (x, y) coordinates on the grating surface. The polynomial expansion coefficients of W_M and W_H are M_{ij} and H_{ij}, respectively. The coefficient M_{ij}, expressed as the expansion coefficient of the (i, j) term, describes how the wavefront diffracted from arbitrary point $P(x, y)$ on the grating toward the ideal image point from an object point. The other term H_{ij} is generalized to account for the image-modifying effects of the variations in curvature and spacing of the grooves. The wavefront from the constant line spacing gratings is dominated by the M_{ij} term, and the H_{ij} term is zero when $(i + j) \geq 2$. While for VLS gratings, the H_{ij} term describes effects of the groove pattern. As a holographic grating, the H_{ij} coefficient can be written in terms of the parameters of the recording geometry,

$$H_{ij} = \frac{m\lambda}{\lambda_0} h_{ij}, \tag{2}$$

where λ_0 is the recording wavelength in the fabrication of holography, m is the diffraction order, and λ is the diffracted wavelength. Although the specific expression of the H_{ij} term for ruled gratings is a little different, they can be transformed by each other [14]. In this case, the diffracted wavefront of the holographic gratings is coincident with that from the ruled gratings.

B. Diffracted Wavefront under Littrow Conditions

Various commercial interferometers have been applied for measuring the spherical surface. Generally, we take the Fizeau interferometer for testing layout analysis. In the traditional spherical surface testing, the curvature center of the test surface is ideally positioned to coincide with the curvature center of the reference surface of the transmission sphere. Similarly, positioning a spherical grating following the above criteria allows testing the diffracted wavefront at its 0 order. To measure wavefront from other orders, the grating is tilted about its vertex at a specific angle, which is referred to as the Littrow angle. The Littrow angle for the unique order is derived from the grating equation when autoreflection from the grating surface is acquired for the principal rays. And the Littrow angle is determined by Eqs. (3) and (4) when $\alpha = \beta$,

$$d_v(\sin\alpha + \sin\beta) = m\lambda, \tag{3}$$

$$\theta_L = \sin^{-1}\left(\frac{m\lambda}{2d_v}\right), \tag{4}$$

where d_v is the groove spacing at the vertex of spherical gratings, α is the incident angle, β is the diffraction angle, and θ_L is the Littrow angle. As shown in Fig. 1, the concave grating is

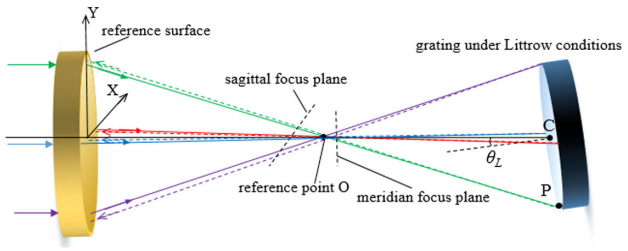

Fig. 1. Spherical grating test under Littrow conditions.

placed at the Littrow angle, point O is the focus of the reference surface, point C is the vertex of the grating, and the distance between point O and C is equal to the radius of the grating. In this instance, the diffracted wavefront at the point O can be expressed as

$$\begin{aligned}\mathrm{OPD} &= 2(|OP| - |OC|) + m\lambda N \\ &= \sum_{i=0}^{\infty}\sum_{j=0}^{\infty}(M_{ij}x^i y^j + H_{ij}x^i y^j). \end{aligned} \tag{5}$$

The optical path difference (OPD) is equivalent to the sum of the optical path difference by the substrate and the phase retardation $m\lambda N$ by the grooves. The diffraction order is m. N is supposed to be the groove numbers between the vertex point C and the arbitrary point P on the grating surface.

The M_{ij} term in Eq. (5) is expanded to the sixth order in this paper such that the precision of the calculated wavefront can be as high as $10^{-3}\lambda$ RMS. Since the object distance is equal to the image distance under Littrow conditions, the coefficients M_{ij} can be simplified as

$$M_{20} = \frac{\cos^2\theta_L}{r_{OC}} - \frac{\cos\theta_L}{R}, \tag{6}$$

$$M_{02} = \frac{1}{r_{OC}} - \frac{\cos\theta_L}{R}, \tag{7}$$

$$M_{30} = \frac{\sin\theta_L}{r_{OC}}\left(\frac{\cos^2\theta_L}{r_{OC}} - \frac{\cos\theta_L}{R}\right), \tag{8}$$

$$M_{12} = \frac{\sin\theta_L}{r_{OC}}\left(\frac{1}{r_{OC}} - \frac{\cos\theta_L}{R}\right). \tag{9}$$

Specific expressions are shown in the Appendix A. Deducing from Eqs. (6) and (7), M_{20} and M_{02} cannot be zero simultaneously. Astigmatism is the dominant aberration in the wavefront diffracted from the spherical grating, for the meridional and sagittal foci are not coincident. When testing a spherical grating under Littrow conditions, the measured wavefront data are composed of an ideally diffracted wavefront as expressed by Eq. (5) and the wavefront error induced by manufacturing imperfections. Consequently, we believe that three issues dominate the construction of the spherical gratings testing configuration for nonnull interferometric testing:

(1) the grating is placed at Littrow angle according to the expected testing order;
(2) the position of the grating along the optical axis has to be located with the point O lies between its meridional and sagittal image plane, where astigmatism is observed as the dominant aberration in the interferogram; and
(3) the ideally diffracted wavefront should be conveniently and precisely removed from the measured data.

3. DUAL MEASUREMENTS WITH OPPOSITE DIFFRACTION ORDERS

A. Components of the Measured Wavefront Data

The diffracted wavefront of the ideal spherical grating placed under nominal Littrow conditions is analyzed in Section 2. However, misalignment of spherical grating is unavoidable in the experimental setup. When testing a spherical surface, the spherical wavefront error induced by the surface figure error is routinely obtained by eliminating the misalignment errors expressed as piston, tilt, and defocus terms from the measured wavefront data. However, other than the misalignment error of the spherical surface, the measured wavefront data also contain the contributions from the groove pattern of spherical gratings. Therefore, the conventional misalignment elimination method needs to be analyzed and discussed.

In addition to the ideally diffracted wavefront analyzed in Section 2, the manufacturing imperfections of a grating will induce wavefront error in the measured wavefront data, and misalignment in the testing configuration will also introduce misalignment aberrations. Therefore, the measured wavefront data are composed of the ideally diffracted wavefront, the wavefront error, and misalignment aberrations. The ideally diffracted wavefront is further divided into substrate surface contributions induced by geometry of the testing configuration and groove pattern contributions. The wavefront error induced by manufacturing imperfections of the grating is the component we care about, which should be precisely extracted from the measured wavefront data. Without loss of generality, the components of the measured wavefront data of a holographic grating are expressed as

$$W_t = W_M + W_H + W_e + W_{\mathrm{mis}}, \tag{10}$$

where W_t is the measured wavefront data. W_M is the substrate surface contributions under Littrow conditions. It contains two parts. One of them is the figure of substrate, which could be measured at 0th diffraction order. The other part is aberration caused by changed substrate posture. The latter could be calculated using the M_{ij} term. W_H is the groove pattern contributions, W_e is the wavefront error, and W_{mis} is the misalignment aberrations.

B. Wavefront Error Extraction with Unknown Groove Pattern

According to the analysis of wavefront error testing under Littrow conditions, the wavefront error can be extracted from the measured data by removing ideally diffracted wavefront and misalignment aberrations. However, the expression of the groove distribution is specific for gratings with different processing methods. For a holographic grating, the groove distribution is determined by recording geometry during the fabrication process, while for a ruled grating, the groove distribution is an

infinite polynomial in its projection plane. Thus, the calculation of groove pattern contributions needs the specific equation of the groove distribution and complicated calculations. Moreover, there are some replicated gratings only known by the parameters of radius of curvature, effective aperture, and groove density at its vertex, but the groove distributions are unknown. According to the analysis of the diffracted wavefront as Eq. (2), $H_{ij(m=1)} = -H_{ij(m=-1)}$ is obtained such that the groove pattern contributions are contrary for the opposite diffraction orders. The wavefront term W_H can be eliminated by combining two testing results for a grating with dual measurments using opposite diffraction orders, respectively. Since a grating is always working at $+1$ or -1 orders in the spectrometer, the groove pattern contributions can be eliminated by adding Eqs. (11) and (12),

$$W_{t(m=1)} = W_{M(m=1)} + W_H + W_e + W_{\text{mis1}}, \tag{11}$$

$$W_{t(m=-1)} = W_{M(m=-1)} - W_H + W_e + W_{\text{mis2}}, \tag{12}$$

where $W_{t(m=1)}$ and $W_{t(m=-1)}$ are the measured wavefront data at $+1$ and -1 orders, respectively. The diffracted wavefront error can be extracted from the measured wavefront data by subtracting the substrate surface contributions and misalignment aberrations using Eq. (13),

$$W_e = (W_{t(m=1)} + W_{t(m=-1)} - W_{M(m=1)} - W_{M(m=-1)} - W_{\text{mis1}} - W_{\text{mis2}})/2. \tag{13}$$

Figure 2 shows the general procedure for the dual measurements with opposite diffraction orders.

The procedure can be summarized as follows: first, the grating is aligned at its 0th order where the interferogram is a null-fringe status; then the grating is tilted around its vertex with the Littrow angle of the test order; after that, the astigmatic interferogram is acquired by shifting the grating along the axis; meanwhile the wavefront data can be measured, and the axial distance OC is obtained; the above steps are repeated to acquire the data for the opposite order; subsequently, the wavefront term W_M is calculated according to the Eq. (5) and the wavefront error is outputted after removing W_M, piston, tilt, and power terms.

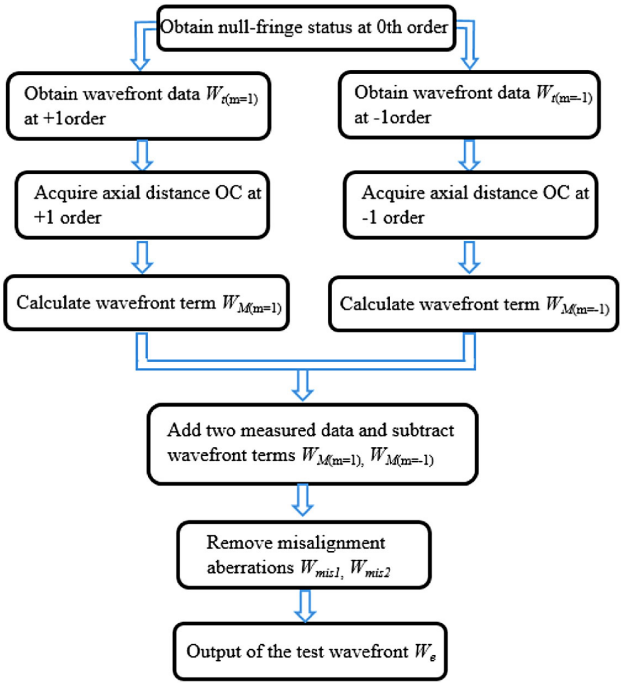

Fig. 2. Procedure for the dual measurements with opposite diffraction orders.

4. SIMULATION

A. Comparison of Traditional Spherical Surface Testing Method and Dual Measurements with Opposite Orders

The test setup in a Fizeau-type interferometer with the working wavelength of 632.8 nm for a VLS concave grating is modeled to analyze the feasibility and precision of the proposed method elaborated in Section 3. Its radius of curvature is 96 mm, the effective aperture is 25 mm, and the groove density at its vertex is 256 lp/mm. The simulated optical configuration is shown in the Fig. 3. Dual measurements are executed by placing the grating at $+1$ and -1 orders under Littrow conditions, respectively.

Figure 4 shows the residual wavefront errors of $+1$ and -1 orders by removing piston, tilt, defocus, and dominant astigmatism terms with the traditional spherical surface testing method. The results by measuring the grating working at $+1$ order and -1 order, respectively, and subtracting the substrate surface contributions with Eq. (13) are illustrated in the Fig. 5.

According to the Fig. 4, the residual PV values are 7.0574λ and 6.9989λ, and the RMS values are 1.0301λ and 1.0230λ applying the traditional method at $+1$ order and -1 order, respectively. The dominant residual error is coma-induced by

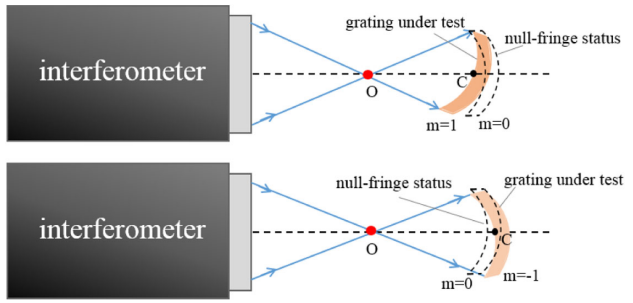

Fig. 3. Schematic of concave grating testing at its $+1$ and -1 orders.

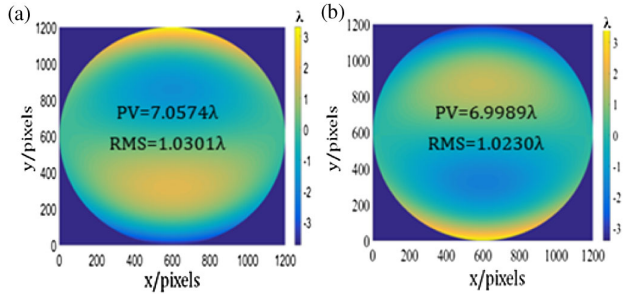

Fig. 4. Residual error with traditional testing method in simulation: (a) at $+1$ order; (b) at -1 order.

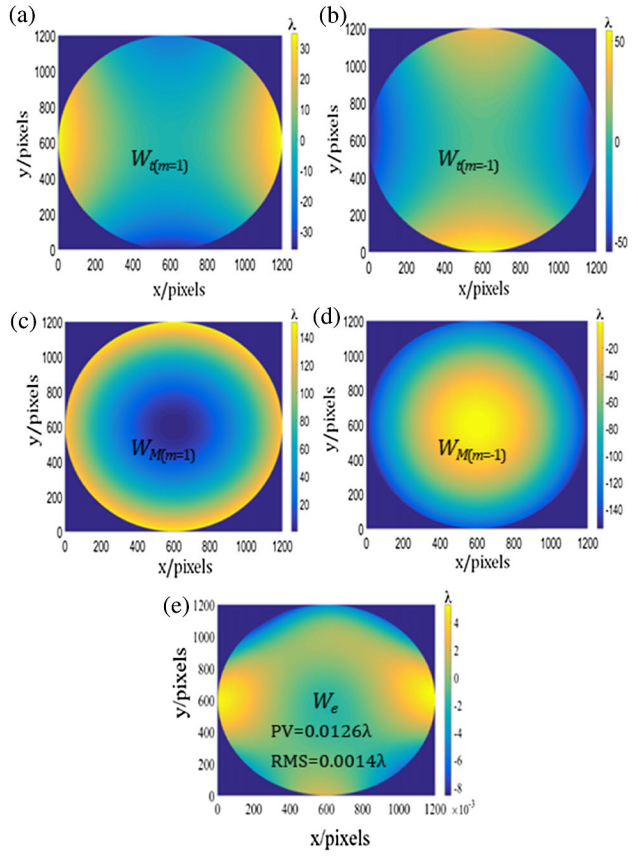

Fig. 5. Simulation with dual diffraction order wavefront measurement method: (a) diffracted wavefront at +1 order; (b) diffracted wavefront at −1 order; (c) calculated wavefront term at +1 order; (d) calculated wavefront term at −1 order; (e) residual error in simulation.

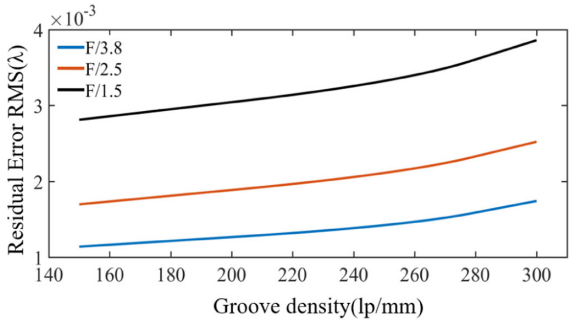

Fig. 6. Simulation for gratings with various NA and groove density.

the groove pattern contributions of the grating that impact the measuring results. While in Fig. 5(e), the PV value of the residual error is 0.0126λ, and RMS = 0.0014λ is obtained. More simulations are implemented for spherical gratings with the F-number slower than 1.5 and the groove density varying from 150 to 300 lp/mm. The results are plotted in Fig. 6 such that the residual wavefront error of the proposed method is less than 0.004λ RMS, validating the feasibility of the method we proposed.

B. Analysis of Misalignment Aberrations

For the traditional spherical surface measurement, misalignment aberrations can be constrained by adjusting the interferogram to null-fringe status. Whereas for spherical grating testing, the grating has to be tilted around its vertex with a certain angle precisely which is difficult to realize. Thus, we analyzed the misalignment aberrations induced by tilt error and corresponding wavefront aberrations in the test results. When the grating is tilted not exactly around its vertex, the actually tilted grating surface and ideally tilted grating surface are shown in the Fig. 7(a). As C is the vertex of the ideally tilted grating, C' is the vertex of the actually tilted grating; the misalignment can be decomposed into defocus and lateral displacement as shown in Figs. 7(b) and 7(c). In this case, we analyzed the measurement precision in our experiment by just removing the tilt and defocus terms as the misalignment aberrations.

Figure 7(b) shows a small longitudinal displacement of the grating, and d represents the longitudinal shift. According to the illustration in Subsection 2.A, the relative OPD between the actually measured wavefront data and the calculated wavefront using the Eq. (5) can be expressed as

$$\mathrm{OPD}_{\mathrm{mis}} = W_M - W_{M(d)} = \sum_{i=0}^{\infty}\sum_{j=0}^{\infty}(M_{ij} - M_{ij(d)})x^i y^j. \tag{14}$$

Considering M_{20} and M_{02} terms:

$$\begin{aligned} W_{20} + W_{02} &= M_{20}X_m^2 x^2 + M_{02}Y_m^2 y^2 \\ &= \frac{M_{20}X_m^2 + M_{02}Y_m^2}{2}(x^2 + y^2) \\ &\quad + \frac{M_{20}X_m^2 - M_{02}Y_m^2}{2}(x^2 - y^2). \end{aligned} \tag{15}$$

The first term and second term represent power and primary astigmatism terms in Zernike polynomials, respectively.

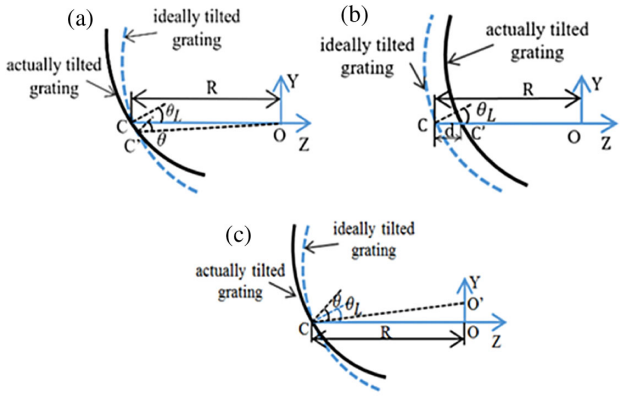

Fig. 7. Misalignment of test spherical grating: (a) tilt; (b) defocus; (c) lateral displacement.

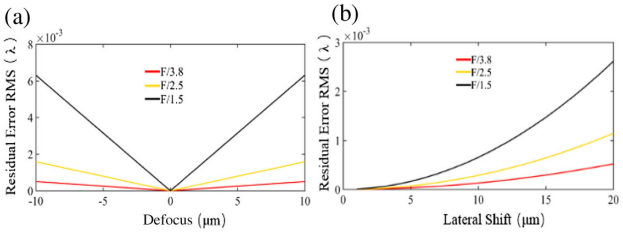

Fig. 8. Residual error in the calibration of misalignment aberrations: (a) RMS values in the calibration of defocus; (b) RMS values in the calibration of lateral shift.

According to the Eq. (15), the astigmatism term Z6 can be calculated as

$$\begin{aligned} Z6 &= \frac{M_{20}X_m^2 - M_{02}Y_m^2}{2} - \frac{M_{20(d)}X_m^2 - M_{02(d)}Y_m^2}{2} \\ &= \left[\frac{\cos^2\theta_L}{r_{OC}} - \frac{\cos\theta_L}{R} - \left(\frac{1}{r_{OC}} - \frac{\cos\theta_L}{R}\right) - \frac{\cos^2\theta_L}{r_{OC}+d}\right. \\ &\quad \left. + \frac{\cos\theta_L}{R} + \left(\frac{1}{r_{OC}+d} - \frac{\cos\theta_L}{R}\right)\right]\frac{Y_m^2}{2} \\ &= (\cos^2\theta_L - 1)\frac{d}{r_{OC}^2 + dr_{OC}}\frac{Y_m^2}{2} \\ &= (\cos^2\theta_L - 1)dNA^2/2, \end{aligned} \tag{16}$$

where $X_m^2 = Y_m^2$ for circular aperture gratings, and the NA can be similarly expressed as $\mathrm{NA} = Y_m/r_{OC}$. According to Eq. (16), the astigmatism induced by misalignment can be neglected when measuring a grating with a small Littrow angle and a low NA. For high-NA gratings the astigmatism term should be removed to calibrate misalignment aberrations.

Figure 8 shows the residual error with different lateral shift and defocus after removing piston, tilt, and power terms as misalignment aberrations. According to Fig. 8(a), the residual error introduced by the wavefront defocus is less than 0.007λ RMS within a 10 μm defocusing amount. From Fig. 8(b), the RMS value of the residual error for the F = 1.5 test grating is less than 0.003λ corresponding to a 20 μm lateral shift amount. The misalignment aberrations induced by the tilt error are the synthetic residual error of lateral shift and defocus. Consequently, the general residual error is less than 0.001λ RMS for gratings with an F-number slower than 1.5. According to the Eq. (16), the astigmatism term should be removed for measuring high-NA gratings. In our simulation, we removed the piston, tilt, and defocus as the misalignment aberrations for the low-NA grating we used. Measurement of high-NA gratings requires further analysis and experimentation.

5. EXPERIMENTAL VALIDATION

In order to verify the feasibility of the dual measurements with opposite diffraction orders, we carried out the experiments utilizing the commercial Fizeau interferometer working at

Table 1. Testing Parameters of the Experiment

	Test at +1 Order	Test at −1 Order
Axial translation distance (mm)	+5.251	−5.730
Tilted angle (°)	+3.61	−3.61

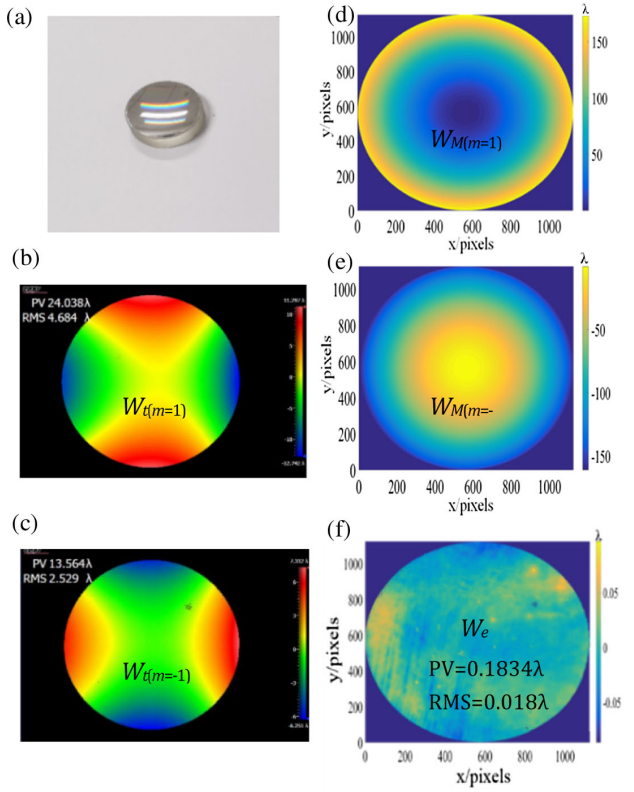

Fig. 9. Measurement result with dual diffraction order measurement method: (a) photograph of the grating; (b) measured diffracted wavefront at +1 order; (c) measured diffracted wavefront at −1 order; (d) calculated substrate surface contributions at +1 order; (e) calculated substrate surface contributions at −1 order; (f) wavefront error with dual diffraction order measurement method.

λ = 632.8 nm. A VLS concave grating, with curvature radius $R = 88.2$ mm, groove density at its vertex $p = 200$ lp/mm, numerical aperture NA = 0.13, and unknown groove pattern, was used for testing the diffracted wavefront. In our experiment, the grating was placed at a null-fringe status as an original position when the grating worked at its 0 order. Then the diffracted wavefront was first measured at its +1 order. The grating was tilted around its vertex according to the Littrow angle and was moved forward along the axial. Second, the grating was measured at its −1 order. The grating was restored to the null-fringe status, then tilted around its vertex according to the Littrow angle, and moved backward along the axial. The tilt angle and axial translation distance relative to the original position are presented in the Table. 1. The precision of the displacement stage used in our experiment is 10 μm, which did not impact the testing result according to the analysis of misalignment aberrations induced by defocus in Fig. 8(a).

The photograph of the tested concave grating is shown in Fig. 9(a). Figs. 9(b) and 9(c) present the measured data at +1 order and −1 order, respectively, in which astigmatism is the dominant aberration. The PV value is 24.038λ and RMS is 4.684λ at +1 order. And the PV value is 13.564λ and RMS is 2.529λ at −1 order. The corresponding substrate contributions based on the experiment setup parameters according to Table 1 are shown in Figs. 9(d) and 9(e). The measured wavefront error after removing substrate surface contributions and misalignment aberrations is shown in the Fig. 9(f). The PV value of the test wavefront error is 0.1834λ, and RMS 0.018λ indicates the fabrication error.

6. CONCLUSION

According to the diffracted wavefront analysis of spherical gratings, the wavefront error test under Littrow conditions suffers from aberrations caused by substrate surface contributions and groove pattern contributions. In order to test gratings without foreknowledge of the groove pattern, we propose a nonnull interferometric testing method under Littrow conditions with opposite diffraction orders. Both the computer simulation and experimental results confirm the feasibility of the proposed method. The analysis of the misalignment aberrations of the measurement demonstrates that the traditional misalignment calibration method is still applicable for low-numerical spherical gratings, while the astigmatism term should be further removed as the residual error for high-numerical spherical gratings. The method achieves high measurement precision, providing a feasible way for spherical grating testing without knowledge of the specific groove pattern.

APPENDIX A: SUBSTRATE SURFACE CONTRIBUTIONS M_{ij} TERMS UNDER LITTROW CONDITIONS

$$M_{20}: \frac{\cos^2\theta_L}{r_{OC}} - \frac{\cos\theta_L}{R}$$

$$M_{02}: \frac{1}{r_{OC}} - \frac{\cos\theta_L}{R}$$

$$M_{30}: \frac{\sin\theta_L}{r_{OC}}\left(\frac{\cos^2\theta_L}{r_{OC}} - \frac{\cos\theta_L}{R}\right)$$

$$M_{12}: \frac{\sin\theta_L}{r_{OC}}\left(\frac{1}{r_{OC}} - \frac{\cos\theta_L}{R}\right)$$

$$M_{40}: \frac{\cos\theta_L}{8R^3} - \frac{\sin^2\theta_L}{8R^2 r_{OC}} - \frac{\cos\theta_L - 3\sin^2\theta_L\cos\theta_L}{4Rr_{OC}^2} - \frac{5\sin^2\theta_L\cos^2\theta_L - \cos^2\theta_L}{8r_{OC}^3}$$

$$M_{22}: \frac{\cos\theta_L}{4R^3} - \frac{\sin^2\theta_L}{4R^2 r_{OC}} - \frac{2\cos\theta_L - 3\sin^2\theta_L\cos\theta_L}{4Rr_{OC}^2} - \frac{1-3\sin^2\theta_L}{4r_{OC}^3}$$

$$M_{04}: \frac{\cos\theta_L}{8R^3} - \frac{\sin^2\theta_L}{8R^2 r_{OC}} - \frac{\cos\theta_L}{4Rr_{OC}^2} - \frac{1}{8r_{OC}^3}$$

$$M_{50}: \frac{7\sin^3\theta_L\cos^2\theta_L - 3\sin\theta_L\cos^2\theta_L}{8r_{OC}^4} + \frac{\sin\theta_L\cos^3\theta_L + 2\sin\theta_L\cos\theta_L}{4r_{OC}^3 R} + \frac{\sin\theta_L - 3\sin\theta_L\cos^3\theta_L}{8r_{OC}^2 R^2} - \frac{\sin\theta_L\cos\theta_L}{8r_{OC}R^3}$$

$$M_{32}: \frac{2\sin^3\theta_L - 3\sin\theta_L\cos^2\theta_L}{4r_{OC}^4} - \frac{\sin\theta_L\cos^3\theta_L + 5\sin\theta_L\cos\theta_L}{4r_{OC}^3 R} + \frac{\sin^3\theta_L - \sin\theta_L\cos^2\theta_L}{4r_{OC}^2 R^2} - \frac{\sin\theta_L\cos\theta_L}{4r_{OC}R^3}$$

$$M_{14}: \frac{-3\sin\theta_L}{8r_{OC}^4} + \frac{\sin\theta_L\cos^3\theta_L + 2\sin\theta_L\cos\theta_L}{4r_{OC}^3 R} + \frac{\sin\theta_L - 3\sin\theta_L\cos^3\theta_L}{8r_{OC}^2 R^2} - \frac{\sin\theta_L\cos\theta_L}{8r_{OC}R^3}$$

$$M_{60}: \frac{\cos^2\theta_L + 7\sin^4\theta_L\cos^2\theta_L - 14\sin^2\theta_L\cos^4\theta_L}{16r_{OC}^5} + \frac{35\sin^2\theta_L\cos^3\theta_L - 85\sin^4\theta_L\cos\theta_L - 6\cos\theta_L}{32r_{OC}^4 R} + \frac{2 - 15\sin^2\theta_L\cos^2\theta_L}{16r_{OC}^3 R^2} + \frac{\cos\theta_L}{16r_{OC}^2 R^3} + \frac{\sin^2\theta_L}{16r_{OC}R^4} - \frac{\cos\theta_L}{16R^5}$$

$$M_{42}: \frac{3 - 5\sin^4\theta_L - 30\sin^2\theta_L\cos^2\theta_L}{16r_{OC}^5} + \frac{55\sin^2\theta_L\cos^3\theta_L - 15\sin^4\theta_L\cos\theta_L - 9\cos\theta_L}{16r_{OC}^4 R} + \frac{3 + 3\cos^4\theta_L - 27\sin^2\theta_L\cos^2\theta_L}{16r_{OC}^3 R^2} + \frac{3\cos\theta_L + \sin^2\theta_L\cos\theta_L}{16r_{OC}^2 R^3} + \frac{3\sin^2\theta_L}{16r_{OC}R^4} - \frac{3\cos\theta_L}{16R^5}$$

$$M_{24}: \frac{3\cos^2\theta_L - 12\sin^2\theta_L}{16r_{OC}^5} + \frac{37\sin^2\theta_L\cos\theta_L - 18\cos^3\theta_L}{16r_{OC}^4 R} + \frac{6\cos^4\theta_L - 9\sin^2\theta_L\cos^2\theta_L}{16r_{OC}^3 R^2} + \frac{3\cos\theta_L + 2\sin^2\theta_L\cos\theta_L}{16r_{OC}^2 R^3} + \frac{3\sin^2\theta_L}{16r_{OC}R^4} - \frac{3\cos\theta_L}{16R^5}$$

$$M_{06}: \frac{1}{8r_{OC}^5} - \frac{3\cos\theta_L}{8r_{OC}^4 R} + \frac{2\cos^2\theta_L - \sin^2\theta_L}{8r_{OC}^3 R^2} + \frac{\cos\theta_L + \sin^2\theta_L\cos\theta_L}{8r_{OC}^2 R^3} + \frac{\sin^2\theta_L}{8r_{OC}R^4} - \frac{\cos\theta_L}{8R^5}$$

Funding. Chinese Academy of Sciences (KLOMT190201); Fundamental Research Funds for the Central Universities (30919011277, 30919011278); National Natural Science Foundation of China (U1931120); National Key Research and Development Program of China (2019YFB2005500).

Disclosures. The authors declare that there are no conflicts of interest related to this paper.

REFERENCES

1. X. Prieto-Blanco, C. Montero-Orille, B. Couce, and R. de la Fuente, "Analytical design of an Offner imaging spectrometer," Opt. Express **14**, 9156–9168 (2006).
2. A. N. Melnikov and E. R. Muslimov, "Analysis of versions of the optical layout of a high-aperture imaging spectrograph based on a convex holographic diffraction grating," J. Opt. Technol. **86**, 153–159 (2019).
3. L. Feng, L. Wei, and Y. Nie, "Design of a compact spectrometer with large field of view based on freeform surface," Opt. Commun. **444**, 81–86 (2019).
4. Z. Li, M. Jamal Deen, Q. Fang, and P. R. Selvaganapathy, "Design of a flat field concave-grating-based micro-Raman spectrometer for environmental applications," Appl. Opt. **51**, 6855–6863 (2012).
5. S. Bonora, F. Frassetto, and E. Zanchetta, "Active diffraction gratings: development and tests," Rev. Sci. Instru. **83**, 123106 (2012).
6. M. R. Gleeson, C. E. Close, F. T. O'Neill, and J. T. Sheridan, "Fabrication and testing of holographic gratings," Proc. SPIE **5521**, 137–148 (2004).
7. C. Palmer, *Diffraction Grating Handbooks* (2002), Vol. **5**, p. 137.
8. S. Morozumi, "Toric-wavefront testing holographic interferometry for concave gratings," Appl. Opt. **23**, 3082–3090 (1984).
9. E. A. Sokolova, V. Kruizinga, D. De Bruijn, and M. Broxterman, "Computer modelling of a wavefront diffracted at a concave grating," J. Opt. Technol. **70**, 600–606 (2003).
10. D. Xu, J. Reimers, J. C. Papa, J. D. Owen, M. A. Davies, T. J. Suleski, K. P. Thompson, and J. P. Rolland, "Testing of a convex reflective diffraction grating," in *Optical Design and Fabrication (Freeform,*

IODC, OFT), OSA Technical Digest (Optical Society of America, 2017), paper OM2B.3.
11. D. Xu, J. D. Owen, J. C. Papa, J. Reimers, T. J. Suleski, J. R. Troutman, M. A. Davies, K. P. Thompson, and J. P. Rolland, "Design, fabrication, and testing of convex reflective diffraction gratings," Opt. Express **25**, 15252–15268 (2017).
12. M. P. Chrisp, "Aberrations of holographic toroidal grating systems," Appl. Opt. **22**, 1508–1518 (1983).
13. S. H. Kim, H. J. Kong, and S. Chang, "Aberration analysis of a concentric imaging spectrometer with a convex grating," Opt. Commun. **333**, 6–10 (2014).
14. C. Palmer and W. R. McKinney, "Equivalence of focusing conditions for holographic and varied line-space grating systems," Appl. Opt. **29**, 47–51 (1990).